MICROSTRIP PATCH RADIATING ELEMENTS FOR CIRCULARLY-POLARIZED PHASED ARRAY

Paul G. Elliot and Mohamed S. Mahmoud[1]
MITRE Corporation, Bedford, MA, 01730 USA
pelliot@mitre.org

ABSTRACT

This report evaluates circularly-polarized single-probe fed microstrip patch radiating elements for a low profile phased array antenna. The design, measurements, and computer modeling results are described for two designs: one is a patent pending dual-slot on each side of the patch, and the other is a conventional single slot design. Antenna requirements also include: 14.40 to 15.35 GHz frequency band, 2 dB axial ratio, and low VSWR with scan. The patches were arrayed with 7 driven elements in an equilateral triangular lattice. Electromagnetic computer models accurately predicted performance. In particular, the measured directivity was extremely close to the computer model prediction, as was the frequency of best axial ratio. However, the computer model usually predicted better axial ratio and wider axial ratio bandwidth than was realized in the measurements.

KEY WORDS: phased-array antennas, microstrip antennas, circular polarization, electromagnetic modeling.

1. Introduction

The circularly polarized (CP) microstrip patch radiating elements described here are for a low profile Ku-band phased array. Patch and array dimensions, measured results, and computer model results are shown and discussed for the two patch designs shown in Figures 1 and 2: one is a patent pending dual-slot on each side of the patch [1], and the other is a conventional single slot design [2,3,4]. Initial requirements of 13.875 to 14.875 GHz and 30° scan for the dual-slot design were updated to the requirements in Table 1 for the single slot design. Table 1 shows a bandwidth of 0.95 GHz (6.4%) centered at 14.875 GHz.

Table 1. Patch Array Performance Objectives

Frequency	14.40 to 15.35 GHz
Polarization	Circular Polarization (CP)
Axial Ratio	2.0 dB
VSWR	1.7:1 (S_{11} < -11.7 dB)
Power Handling	0.5 W per Element
Scan Angle	0-60° Desired

Single-probe fed CP patches were used to avoid a quadrature hybrid for each element. Electromagnetic (EM) computer modeling using Ansoft Designer software [5] was used to help design the patches and arrays. This report discusses the radiating patch elements only. The feed components and additional antenna information is described in several MITRE technical reports (not in public domain).

2. Microstrip Patch Designs

Figures 1 and 2 are drawings (not to scale) of the two patch designs, and Table 2 lists the single patch dimensions. If the feed probe location is rotated by 90° then these patches produce RHCP instead of LHCP.

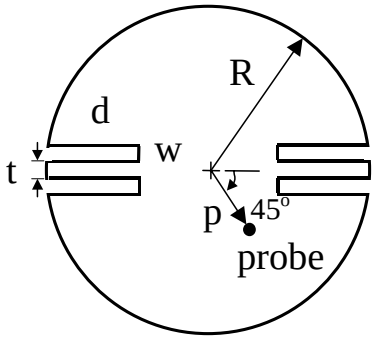

Figure 1. Dual-Slot Patch (Patent Pending)

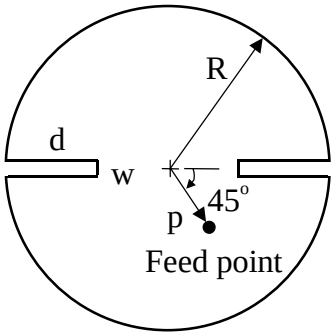

Figure 2. Single-Slot Patch

[1] Mohamed Mahmoud is now at Lockheed-Martin Space Systems Advanced Technology Center, Sunnyvale, California 94089 USA. msamehm@ieee.org

Table 2. Single Patch Dimensions

	Dual-Slot Patch	**Single-Slot Patch**
Patch Polarization	CP	CP
Patch Shape	Circular	Circular
Patch Radius (R)	0.124”	0.138”
Probe Feed Point from Patch Center (p)	0.062”	0.068”
Probe Diameter	0.020”	0.020”
Slot for Producing CP	2 Double Slots	2 Single Slots
• Slot Length (d) • Slot Width • Slot Septum Width (t)	0.074” w = 0.010” (ea) 0.010”	0.046” 0.046” na
Dielectric Substrate	Taconic TLY-3	Taconic TLY-5
• Substrate Thickness • Dielectric Constant • Loss Tangent • Substrate Diameter	0.062 2.33 0.0013 2.40”	0.045” 2.20 0.0009 2.40”
Ground Plane Diameter*	5.14”	5.14”
Patch Metallization	½ oz copper	½ oz copper

* Circular ground plane with rolled edge.

Theoretical methodologies for patch antenna design, and a description of the EM modeling software, are given in the references but cannot be repeated here due to space limitations.

3. Array Parameters

The patch designs described above were also arrayed using 7 driven elements. The array parameters are listed in Table 3. This small array is an initial design step toward a possible larger array. The parameters for the two array designs differ due to the approaches taken by different designers, and since the main objective was to best meet the goals listed in Table 1, which changed a bit over time. The objective was not to make a controlled comparative evaluation of the two patch designs.

Table 3. Patch Array Parameters

	Dual-Slot Patch Array	**Single-Slot Patch Array**
Substrate Diameter	2.40”	3.25”
Array Lattice	Equilateral Triangular	Equilateral Triangular
# Patches Excited	7	7
Dummy Elements	0	12
Total # Patches	7	19
Element Spacing, cm	1.321 cm	1.016 cm
“ “ inches	0.520”	0.400”
“ λ @15.35 GHz	0.676 λ	0.520 λ
Sequential Rotation	No	Yes

The different array element spacing impacts several array performance parameters including the following: the closer spacing for the single-slot array permits scan over a ±60° degree cone, while the dual-slot array can scan over a ±30° cone without grating lobe peaks at the highest frequency. This single-slot array will have less directivity than the same number of elements driven in the dual-slot array by a factor of approximately $(0.400” / 0.520”)^2$ = -2.3 dB. Closer element spacing also reduces the space available for feed components under the elements. Closer spacing generally gives greater mutual coupling, although when scanning this is partially offset by the smaller interelement phase shift required for scan to a given angle. For these tests the antenna was not yet integrated with any of the multilayer feed components, phase shifters, amplifiers etc.

3. Measured and Computer Model Results

For the S-parameter results the reference plane for the patch element ports is at the bottom of the patch probe where it passes through an opening in the ground plane. For the radiation pattern cuts, $\theta = 0$ is the direction normal to the patch surface. All pattern cuts shown here are $\phi = 0$ cuts, which is parallel to the line passing through the notches on each side of the center patch. Other pattern cuts are not shown due to space limitations.

3.1 Isolated Patch Results

Figures 3 and 4 compare the measured S11 traces with the EM computer model S11 results for both patch designs. These are for isolated patches, i.e. one patch only etched on the substrate, not in an array. The Smith chart traces start at 12 GHz at the upper-right end of the trace and follow an overall clock-wise direction as the frequency increases as do most passive devices, ending at 18 GHz. A thick substrate was used to increase VSWR bandwidth: the VSWR is below 2:1 from about 14 to 16.5 GHz for these curves. The input impedance seen in Figures 3 and 4 is inductive at most frequencies. The probe contributes an inductance, especially for these thick substrates which results in long probe. So it was necessary to also use a relatively thick probe (0.020”) to reduce inductance.

In Figure 3, the EM model results shows a “kink” at 14.6 GHz, and for the measured trace the kink was less pronounced but also at 14.6 GHz $\pm$ 0.2 GHz. This kink frequency should theoretically yield the best axial ratio for a single-probe CP patch due to the combination of mode resonances [2,3,6,7], and not coincide exactly with lowest VSWR frequency. These predictions are borne out by the single-slot results shown in Figures 3 and 5.

In Figure 4, the EM model shows a kink centered at 14.5 GHz, however the two measured traces in Figure 4 do not as clearly show the typical “ω“ shaped trace, so they do not show a single clear kink frequency. Also there is considerable variation between the two measured

curves in Figure 4 which are the same design. These problems are most likely due to the coax outer-conductors being soldered directly to the ground plane; at these Ku-band frequencies that solder joint was probably causing an unpredictable and highly variable input reactance. Having seen this happen with the dual-slot patches, the single-slot patches (Figure 3) then used SMA panel or threaded connectors to connect to the ground plane to obtain more repeatable input impedance.

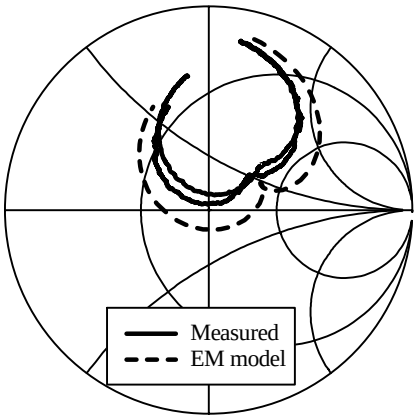

Figure 3. Isolated Patch S11, 12-18 GHz
(Single Slot Patches)

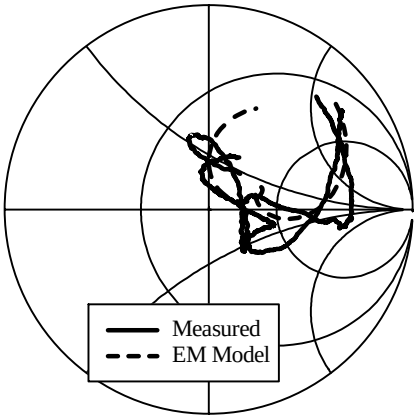

Figure 4. Single Isolated Patch S11, 12-18 GHz
(Dual-Slot Patches)

Figure 5 plots measured Axial Ratio (AR) vs. frequency for these single isolated patches, in the direction normal to the patch surface (boresight). It shows that the best measured axial ratio is at the frequency as predicted by the kink in the Smith charts. Published literature often gives a % bandwidth over which the boresight axial ratio is 3 dB or better. This can be determined from Figure 5: The dual-slot patches both show Axial Ratio ≤ 3 dB Bandwidth (AR 3 dB BW) of 4.4%. The single-slot patch shows 3.4%.

Figures 6 and 7 show the measured isolated patch far-field patterns. The top curve in each of Figures 6 and 7 is the co-polarized (desired sense) CP gain, the middle curve is axial ratio, and the bottom curve is cross-polarized CP. The measured gain includes some loss in the feed coax. Figures 6 and 7 show only the frequency of best axial ratio. Patterns at other frequencies in the band similarly showed a co-polarized pattern with a wide peak with some ripple, and the axial ratio also ripples but usually stays between 0–5 dB out to ±50° scan over most of the desired band.

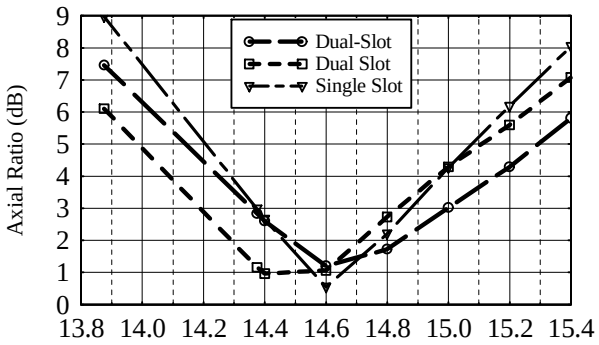

Figure 5. Measured Axial Ratio for Single Isolated Patches in Boresight Direction

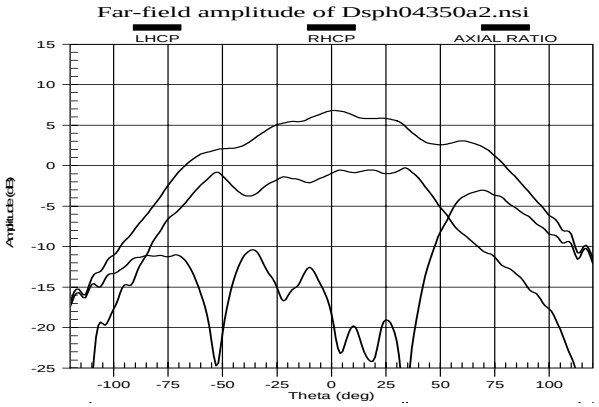

Figure 6. Dual-Slot Isolated Patch Measured Pattern 14.4 GHz

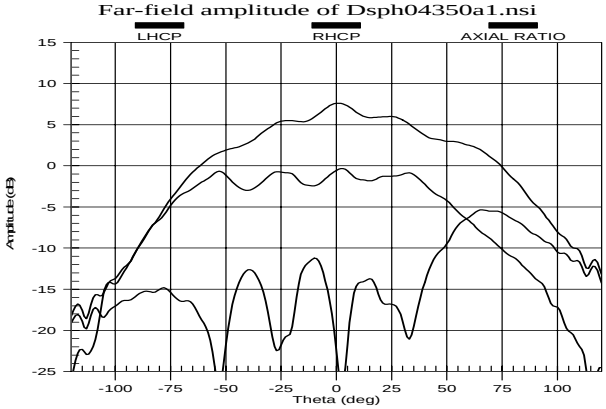

Figure 7. Single-Slot Isolated Patch Measured Pattern, 14.6 GHz

3.2 Array Results

For the arrays, first just the center element was driven with the nearest 6 elements terminated in a 50-ohm resistive load (Section 3.2.1) to see the element performance in the array environment. Then 7 elements of the array were all driven (Section 3.2.2). 50-ohm sources were used to drive the elements. For the single-slot patch array only there was, in addition, an outer ring of 12 elements which were open-circuited for all tests because there was insufficient space to connect loads but it was felt that including them would still help the central elements to see more of a larger array scattering effects.

3.2.1 Center Element of Array Driven

Figures 8 and 9 plot S11 for the central element of the array, with the 6 nearest elements terminated in 50 ohms. In Figure 8 the measured and the computed EM model traces agree closely with regard to the frequency of the small loop, which is from 14.3 GHz to 15.1 GHz, with the center of the loop at 14.6 GHz. The kink in Figure 3 has therefore stayed at the same frequency (centered on 14.6 GHz) but has widened into the small loop in Figure 8. A small loop in the Smith chart for this type of patch normally indicates poorer axial ratio than a sharp kink at one frequency, but also usually indicates a broadening of the axial ratio bandwidth (albeit with a worse axial ratio at the center frequency). This effect is seen here to a small extent, by comparing Figures 5 and 10.

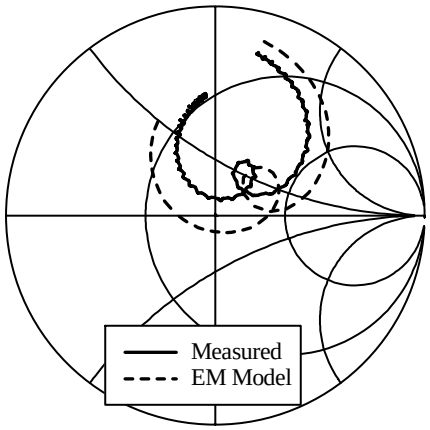

Figure 8. Array Center Patch S11, 12-18 GHz (Single-Slot Patch)

In Figure 9 the EM model shows a kink at 14.4 GHz, but the measured trace does not clearly show which is the kink frequency, probably due to the Ku-band solder joint problem alluded to earlier. Figure 10 plots measured Axial Ratio (AR) vs. frequency for the center element pattern in the direction normal to the patch surface. The best AR is again at the frequency predicted by the kink or small loop in the Smith chart. The AR 3 dB BW is 5.4% for the dual-slot patch and 4.7% for the single-slot. The element pattern (not shown) is narrower than for the isolated patch, especially for the single-slot patch, this would reduce gain at wide scan angles.

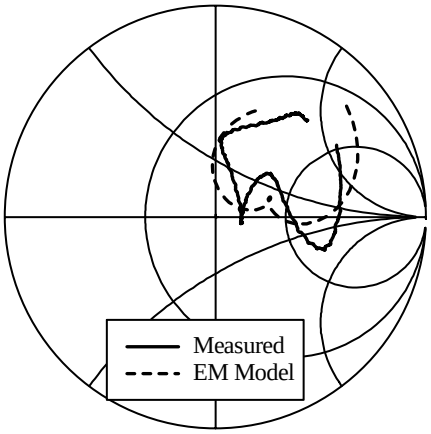

Figure 9. Array Center Patch S11, 12-18 GHz (Dual Slot Patch)

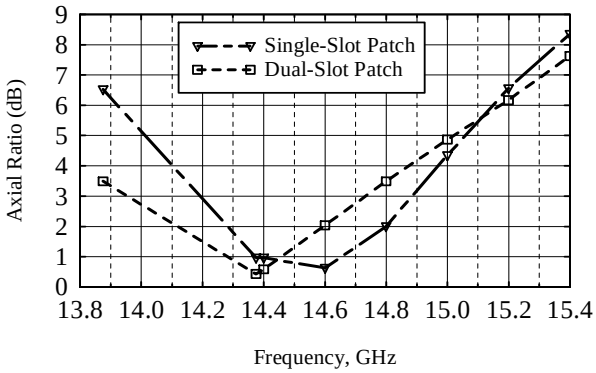

Figure 10. Measured Axial Ratio for Center Patch of Array, in Broadside Direction (Only) One Patch Driven

3.2.2 Array with 7 Elements Driven

Figures 11 through 14 plot the reflection coefficient Γ for the center patch when all 7 central patches are excited and driven, computed from the following formula:

$$\Gamma_m(\theta) = \sum_{n=1}^{N} S_{mn}\, a_n / a_m \quad , \qquad (1)$$

where $\mathbf{S_{mn}}$ are the S-parameters for the element ports, either measured or from the EM model as indicated for each curve in the figure. Subscript **m** designates the port number for which we compute $\mathbf{\Gamma}$, in this case the center element. The $\mathbf{a_n}$ and $\mathbf{a_m}$ are the complex driving excitations (forward voltages) at each element port, phased for the desired beam direction $\boldsymbol{\theta}$ of the array. Figures 11 and 12 plot Γ for the broadside beam ($\boldsymbol{\theta} = 0$). These differ from Figures 8 and 9 due to energy coupled into the center patch from the 6 contiguous patches, which occurs for Figures 11 and 12 but not Figures 8 and 9. In Figure 11 there are two kinks or loops; one is 14.4 to 14.6 GHz, and the smaller kink at 15.3 GHz. The best axial ratio was found at 14.6 GHz. In Figure 12 the kink

in the EM model seen earlier in Figure 9 has widened into a loop from 14.1 to 15.8 GHz, as mentioned earlier this typically indicates poorer axial ratio than a sharp kink at one frequency but also a broadening of the axial ratio bandwidth.

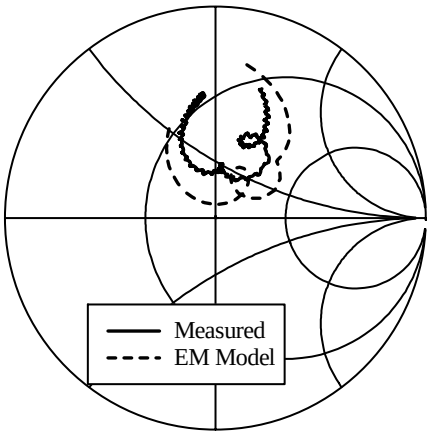

Figure 11. Array Center Patch Γ, 12-18 GHz
With 7 Elements Driven for Broadside Beam
(Single Slot Patch Array)

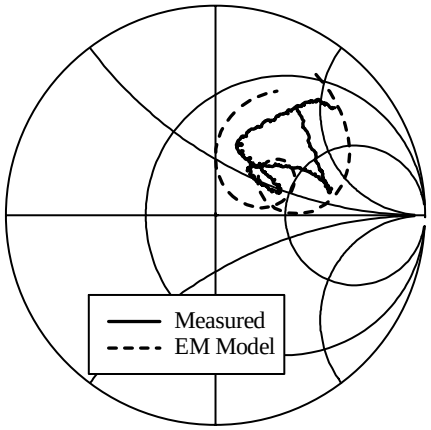

Figure 12. Array Center Patch Γ, 12-18 GHz
With All 7 Elements Driven for Broadside Beam
(Dual Slot Patch Array)

Figures 13 and 14 show $|\Gamma|$ in dB when the beam is scanned to numerous directions covering an entire conical scan region. These were computed using the measured S-parameters and Eq. (1), with the $\mathbf{a_n}$ phased for scan in hundreds of different scan directions within the $\theta < 30$ scan cone. The top of the dark region therefore shows the worst case mismatch ($|\Gamma|$ or Return Loss) with 7 elements driven for 30° scan in numerous directions. These results are affected by S11 and mutual coupling, and therefore by array spacing as discussed earlier.

The array patterns were then measured with 7 elements driven simultaneously and phased for broadside. Figure 15 plots the Axial Ratio (AR) vs. frequency. For the dual-slot array the best AR is at the frequency predicted by the loop in the Smith chart. For the single-slot array the AR shows a very flat response with frequency obtained by sequential rotation. The measured AR 3 dB BW is 5% for the dual-slot array and over 13% for single-slot with sequential rotation. The AR 2 dB BW is 3.5% for the dual- slot array and the same for the single-slot array.

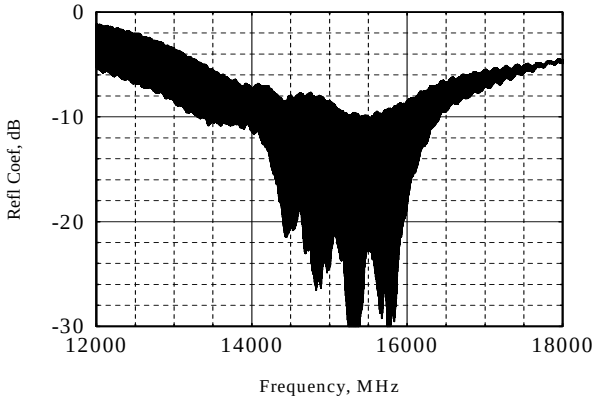

Figure 13. Array Center Element Reflection Coefficient
With 7 Elements Driven Over ± 30° Scan Cone
(Single-Slot Patch Array)

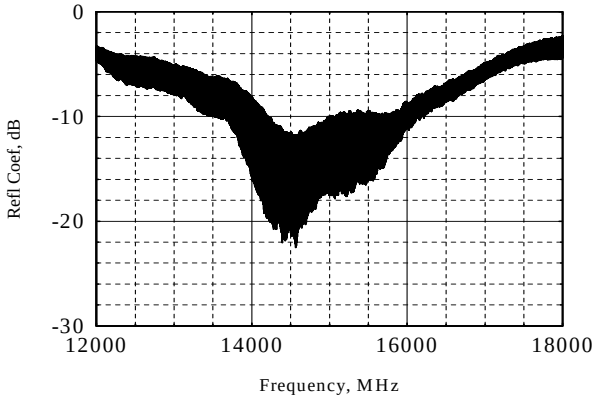

Figure 14. Array Center Element Reflection Coefficient
With All 7 Elements Driven Over ± 30° Scan Cone
(Dual-Slot Array)

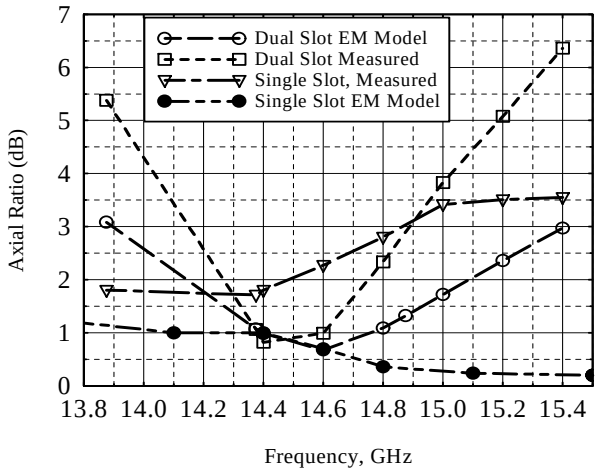

Figure 15. Measured Axial Ratio at Broadside for Array,
7 Elements Driven for Broadside Beam

The design goal was 2 dB AR over the full 6.4% array bandwidth, so for this single-slot array the AR needs to be improved over the top half of the band, and the dual-slot array would also need sequential rotation. As can be seen in Figure 15 for both arrays, the EM model predicted a better AR and a wider AR bandwidth than was realized in the measurements, although the EM model is accurate in predicting the frequency of best AR, and is not far off the value of the AR obtained at that frequency.

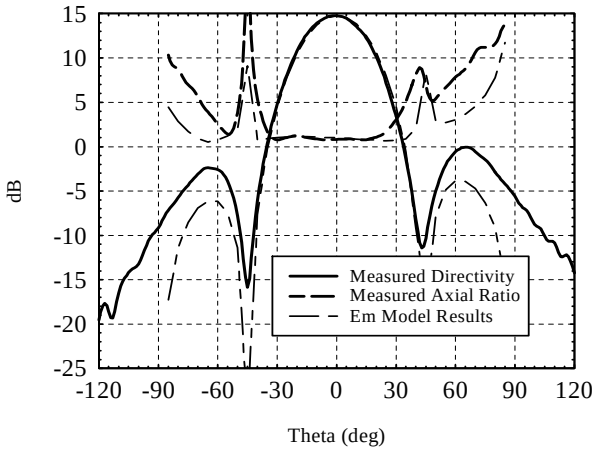

Figure 16. Array Far Field CP Pattern at 14.4 GHz
All 7 Elements Driven for Broadside Beam
(Dual-Slot Patch Array)

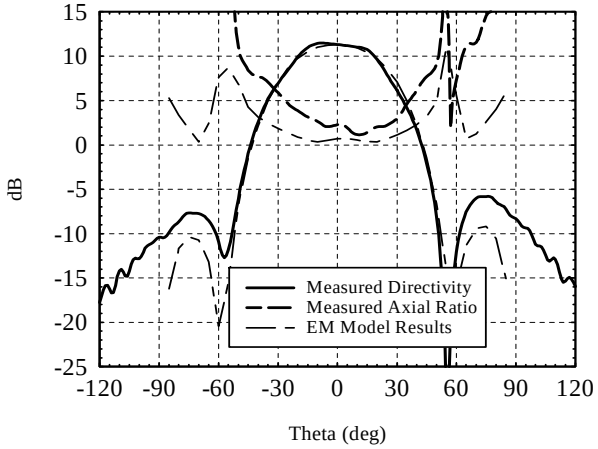

Figure 17. Array Far Field CP Pattern at 14.6 GHz
7 Elements Driven for Broadside Beam
(Single-Slot Patch Array)

Figures 16 and 17 overlay CP directivity and axial ratio for a measured and EM model pattern cut at the frequency with the best axial ratio. The close agreement between the EM computer model and the measured patterns is evident at this frequency. The measured directivity near the peak is extremely close to the EM model prediction (<<1% error for Figure 16 and 1½ % for Figure 17). The measured peak directivity was computed automatically by the near-field range measurement software [8] from a sampling of the entire upper hemisphere of the measured spherical pattern. The single-slot array (Figure 16) shows 3.5 dB lower directivity than the dual-slot array (Figure 17) for both the measured and EM model results. This is partially due to the closer element spacing as mentioned earlier which predicts 2.3 dB lower directivity based on element cell area. The remaining difference is apparently due to sequential rotation, or to the open-circuited dummy elements, or some other difference in the geometry. This could be investigated using the EM model. It is very unlikely to be due to a loose connector since the EM Model also predicted exactly 3.5 dB less gain at that frequency. The amplitudes and phases through the combiner with cables was checked and found to be correct to within ± ½ dB and ±17 deg.

4. Conclusions

The arrays performed well as seen in Figures 16 and 17, forming a directive beam, axial ratio below 1 dB at the best frequency, and VSWR below 2:1 over the band at most scan angles as seen in Figures 13 and 14. The patent- pending dual-slot patch has a 3 dB axial ratio bandwidth of 4.4% for the isolated element and 5% for the 7-element array without sequential rotation. Sequential rotation will be needed to achieve the desired axial ratio over the full bandwidth of the array for these single probe patch designs. The measurements confirmed that a "kink" in the Smith chart impedance plot predicts the frequency with best radiated axial ratio. Electromagnetic computer models using Ansoft Designer software were found to provide a very accurate prediction of this "kink" frequency in the Smith chart, and also a very accurate prediction of the measured peak directivity at that frequency. However the computer model predicted better axial ratio and wider axial ratio bandwidth than was realized in most of the measurements. A thick substrate and wide probe was used to increase VSWR bandwidth.

5. Acknowledgement

This work was supported by U.S. Air Force Contract FA8721-04-C-0001: "Enabling Technologies for Mobile Communications." The measurements were performed by Eddie Rosario of MITRE.

References:

[1] M. S. Mahmoud, "Method and System for a Single-Fed Patch Antenna Having Improved Axial Ratio Performance (AKA Microstrip Antenna Having Slots)." Patent Applic. #10/983,603, filed 9 Nov. 2004.

[2] G. Kumar and K. P. Ray, *Broadband Microstrip Antennas*. Boston: Artech House, 2003.

[3] R. Garg, P. Shartia, I. Bahl, and A. Ittipiboon, *Microstrip Antenna Design Handbook*. Boston: Artech House 2001.

[4] James, Hall and Wood, *Microstrip Antenna Theory and Design*. London: Peter Peregrinus, 1981, pp. 75-86.

[5] *Ansoft Designer* v.2, www.ansoft.com. Initial results were also similar using IE3D of www.zeland.com.

[6] Y. T. Lo and S. W. Lee, *Antenna Handbook*. NY: Van Nostrand Reinhold, 1993, Vol. II. Chapter 10

[7] Hirasawa and Haneishi, *Analysis and Design of Small and Low-Profile Antennas*. Boston: Artech House, 1992. Sect. 4.5.

[8] *NSI 2000*, v4.0. www.nearfield.com.